ACS OMEGA

Open Access

http://pubs.acs.org/journal/acsodf

Article

Proteome Alterations and Nucleosome Activation in Rat Myoblasts Treated with Cerium Oxide Nanoparticles

Andrea Degl'Innocenti,*,# Clarissa Braccia,# Giada Graziana Genchi,▽ Nicoletta di Leo,▽ Luca Leoncino, Federico Catalano, Andrea Armirotti,* and Gianni Ciofani*

Cite This: *ACS Omega* 2024, 9, 29226−29233

Read Online

ACCESS | Metrics & More | Article Recommendations | Supporting Information

ABSTRACT: Oxidative stress is a widespread causative agent of disease. Together with its general relevance for biomedicine, such a dynamic is recognizably detrimental to space exploration. Among other solutions, cerium oxide nanoparticles (or *nanoceria*, NC) display a long-lasting, self-renewable antioxidant activity. In a previous experiment, we evaluated oxidative imbalance in rat myoblasts in space, aboard the International Space Station, and unveiled possible protective effects from NC through RNA sequencing. Here, we focus on the myoblast response to NC on land by means of proteomics, defining a list of proteins that putatively react to NC and confirming nucleosomes/histones as likely mediators of its molecular action. The proteomics data set we present here and its counterpart from the space study share four factors. These are coherently either up- (*Hist1h4b*) or down-regulated (*Gnl3*, *Mtdh*, *Trip12*) upon NC exposure.

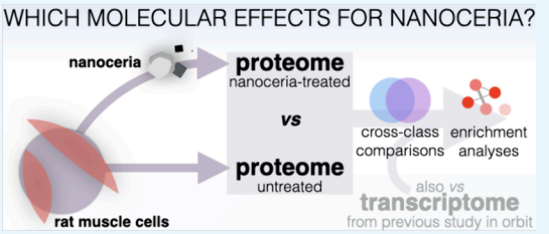

INTRODUCTION

Oxidative stress (OS) is defined as the accumulation of prooxidative agents, chiefly reactive oxygen species (ROS), produced during cellular metabolic activities. Radical buildup can lead to macromolecular damage,[1] causing various pathologic conditions. Instances comprise cardiovascular diseases,[2] premature aging,[3] musculoskeletal disorders,[4] neurodegenerations,[5] and cancer.[6] To counteract the OS, antioxidants can be ingested. These may be either part of a proper diet—for example, ascorbic acid (vitamin C), α-tocopherol (vitamin E), and flavonoids—or uptaken as drugs, like acetylcysteine.[7] Depending on the applications, the rapid clearance of conventional antioxidants might render their use unpractical in the long term. Together with organic antioxidants, radical-scavenging catalysts are among the endogenous defenses of organisms against OS. Some are single detoxifying enzymes such as catalase, superoxide dismutase, or peroxiredoxin. Others take the form of multiplex machineries, like the thioredoxin system (thioredoxin and thioredoxin reductase) or the glutathione system (glutathione, glutathione reductase, and glutathione peroxidase).[8] Exploiting such self-renewable antioxidants as a remedy against OS is possible[9,10] but somewhat troublesome. In fact, they are normally hard to produce/purify in adequate quantities, and their complex organic nature tends to make them perishable or unusable outside of their natural microenvironment. Furthermore, they are often too bulky to move across biological compartments.

As a stable, inorganic, biocompatible compound with proven long-lasting antioxidant properties, cerium oxide nanoparticles (NPs), or *nanoceria* (NC), are a promising alternative to organic antioxidant metabolites and enzymes for the treatment of OS.[11]

The antioxidant properties of NC have been demonstrated in a wide range of biomedical applications. Several studies support relevant pharmaceutical properties against ROS-induced pathologies, including cardiomyopathies. The cardiovascular system is affected by OS, which can lead to ischemic stroke.[12] NC exerts cardioprotective activity thanks to a convenient Ce^{3+}/Ce^{4+} ratio and NP size that together give it the capability to liberate and replenish intracellular oxygen, inducing angiogenesis. Such activity has been described, among others, in murine models of cardiomyopathy, slowing the progression of the disease by attenuating OS.[13−15] The ability of NC to switch between oxidation states III and IV depending on local chemical conditions is the basis of its enzyme-like antioxidant capabilities, fundamental to ensuring a durable action.[16] Consequently, NC holds potential for those situations in which a constant supply of antioxidants is difficult such as in remote outposts. Our group, in particular, proposed that the long shelf life and protracted efficacy of NC make it interesting for the exploration of space, where refurbishment is problematic. The issue is expected to impact future venturing

Received: December 5, 2023
Revised: May 28, 2024
Accepted: June 18, 2024
Published: June 27, 2024

beyond Earth orbit significantly to the point that several space agencies have identified drug storage in space as an open technological challenge. OS is pervasive during space missions, brought about by cosmic radiation, gravity alterations, pressure changes, and confinement. There, the ROS imbalance is recognized as one of the principal causative agents of disease.

While the therapeutic value of NC is widely recognized, its molecular action, either *per se* or in relationship to space travel, is far from being adequately characterized. In a previous work, partially carried out aboard the International Space Station (ISS), we explored the metabolic impact of NC through transcriptomics on rat myoblasts. In that occasion, several differentially expressed genes (DEGs) were identified and two were pinpointed as the most promising candidate NC-responsive genes. These, namely, *lamin A/C* (*Lmna*) and *H2A histone family member X* (*H2afx* or *H2ax*), are both known to have a protective role against OS.[17] To validate such results, and generally as a further step toward the characterization of the molecular dynamics through which NC exerts its biological action, here, we present an on-land proteomics analysis of rat myoblasts, cultured with or without NC—in conditions matching those of ground samples for the ISS study.[17]

METHODS

Preparation and Characterization of Nanoparticle Dispersions. NC (Sigma-Aldrich, 544841) was dispersed at a concentration of 20 mg/mL in sterile ultrapure Milli-Q water by ultrasonication at 8 W for 3 min with a Bandelin ultrasonicator and then incubated with 50% fetal bovine serum (FBS, Sigma-Aldrich, F4135) for 30 min under mild shaking. Subsequently, 1 mg/mL NC dispersions in CO_2-independent medium (Gibco, 18045088) added with 5% FBS were obtained. Immediately before administration to cell cultures, dispersions were further diluted to a final concentration of 100 μg/mL in a CO_2-independent medium, added with 1% FBS, 1% insulin−transferrin−sodium selenite mixture (Sigma-Aldrich, I3146), 2 mM L-glutamine (Gibco, 25030149), and 100 U/mL penicillin−100 μg/mL streptomycin (Pen/Strep, Gibco, 15140122).

For the characterization of dispersions, hydrodynamic diameter (HD), polydispersity index (PDI), and ζ-potential were measured through dynamic light scattering on a Malvern Instruments Zetasizer NanoZS90 tool, at 25 °C. For HD and PDI, dispersions were diluted in complete medium using 25 mM HEPES high-glucose Dulbecco's modified Eagle's medium (DMEM) without phenol red (Sigma-Aldrich, D6171) at 100 μg/mL. In turn, ζ-potential measurements were performed on 100 μg/mL NC dispersions in ultrapure Milli-Q water. HD and ζ-potential values are reported as the mean ± standard deviation of three replicates, each with 13 readings.

In addition, transmission electron microscopy (TEM) was performed on FBS-coated NPs, which were dispersed in ultrapure Milli-Q water at a final concentration of 100 μg/mL, by dropping 2 × 7.5 μL on ultrathin carbon film on copper grid, drying at room temperature on an inverted tweezer, with an adsorption time of 10 min. Samples were stained for 5 min with a solution of 1% uranyl acetate in ultrapure Milli-Q water. Imaging was performed in bright-field modality with two transmission electron microscopes, namely, a JEM-1011 (JEOL), set at 100 kV, and a Tecnai G2 F20 Tween TMP (Schottky emitter), operated at 200 kV. Due to the negative staining, FBS coating of NPs was evaluated by means of contrast.

Cell Culture. H9c2 rat myoblasts (ATCC, CRL 1446)—the same line as for our previous ISS investigation—were routinely cultured (four samples per class) at 70% confluence in 10 mm cell-culture-treated Petri dishes. Once passages 6−12 were reached, H9c2 myoblasts were seeded at a density of 35,000 cells/cm^2 on 90 mm Petri dishes, each containing a silicone ring defining an inner culture chamber of 60 mm in diameter and a height of 6 mm. Such assemblies had been fabricated beforehand, by casting of polydimethylsiloxane (Dow, Sylgard 184) mixed at a ratio of 20:1 w/w with its curing agent around a cylindrical mold, positioned at the center of a 90 mm Petri dish, and then curing the obtained silicon at 60 °C for 2 h, and finally removing the mold to expose the cell-adhesive bottom of the dish. Cell seeding was done with proliferative medium having the following composition: 25 mM HEPES high-glucose DMEM, supplemented with 10% FBS, 2 mM L-glutamine, 1 mM sodium pyruvate, and Pen/Strep. Cultures were kept in an incubator set at 37 °C for 12 h to promote cell adhesion, and then proliferative medium was refreshed (final volume: 16 mL). Cell cultures were sealed with transparent adhesive foil (Bio-Rad, MSB1001) that had been previously exposed to UV light for 20 min. Such adhesive foil was attached to the rim of the silicone ring, and the spaceflight simulation started under normal gravity. This simulation program was introduced to match the growing conditions of ground controls for the ISS study. The latter, indeed, were themselves subjected to a culture program recapitulating treatment schedules and temperature profiles experienced by space samples during their orbital mission.[17]

Spaceflight Simulation under Normal Gravity. In order to simulate cell culture upload to the ISS, myoblasts were exposed for ∼100 h to various temperatures, comprising between 33 and 27 °C, replicating thermal variations that had been experienced by samples during the actual spaceflight.[17] In this time frame, proliferative cell culture medium was not refreshed, as the decreasing temperature had been previously verified to slow down cell proliferation and nutrient exhaustion. To mimic the start of the spaceflight experiment, namely, when space samples reached their incubator aboard the ISS, cell cultures were then administered a differentiative medium (time point identified as t_0) and temperature was increased and held at 37 °C until experiment completion. Differentiative cell culture medium was composed of CO_2-independent medium (Gibco, 18045088), supplemented with 1% FBS, 1% insulin−transferrin−sodium selenite mixture, 2 mM L-glutamine, and Pen/Strep, either added or not with NPs. All cultures were supplied with a differentiative medium without NC at $t_1 = t_0 + 24$ h, and $t_2 = t_0 + 48$ h. After each medium refresh, cultures were carefully sealed with adhesive foil to prevent gas exchanges with the environment. At $t_3 = t_0 + 72$ h, cell cultures were rinsed with phosphate-buffered saline without Ca^{2+} and Mg^{2+} (Gibco, 14190250), trypsinized, and pelleted by centrifugation at 700g for 5 min. Following such first centrifugation, cells were resuspended in phosphate-buffered saline and again centrifuged to remove any traces of proteins in solution.

Total Protein Quantification. Immediately after centrifugation, each cell pellet was lysed in 200 μL of radioimmunoprecipitation assay buffer (RIPA, Sigma-Aldrich, R0278), added with antiproteases (1:1000 diluted, Millipore,

https://doi.org/10.1021/acsomega.3c09715
ACS Omega 2024, 9, 29226−29233

539134) and antiphosphatases (1:50 diluted, Millipore, 524629). Complete lysis was achieved by incubation on ice for 15 min and by vortexing every 5 min. Lysate clarification was obtained by low-temperature centrifugation (4 °C) at 16,000*g* for 20 min. Quantification of total protein content of the samples was then conducted with bicinchoninic acid assay (Thermo Scientific, Pierce 23227) by following the manufacturer's instructions. Finally, the lysates were stored at −80 °C until further usage.

Protein Digestion. An aliquot containing 100 μg of protein was collected from each sample to be digested. Disulfide bonds were first reduced with 10 μL of 100 mM dithiothreitol at 56 °C for 30 min and then alkylated with 30 μL of 100 mM iodoacetamide for 20 min in the dark. Proteins were precipitated in cold (−20 °C) acetone and kept overnight at −20 °C. To remove acetone, a centrifugation step at 20,000*g* for 30 min at 4 °C was performed. The supernatant was discarded, and protein pellets were dried under a nitrogen stream. Dried pellets were dissolved in 200 μL of digestion buffer (ammonium bicarbonate 50 mM in ultrapure Milli-Q water, pH = 8), and then proteins were digested with 2 μg of trypsin overnight at 37 °C. Resulting peptides were dried under vacuum for further analyses.

Creation of the Ion Library. Tryptic peptides were dissolved in 200 μL of 3% acetonitrile + 0.1% formic acid. From each sample, 150 μL was collected and such volumes were pooled together to perform an offline peptide fractionation, following the high pH/low pH strategy.[18] Peptide fractionation was performed using an Oasis solid-phase extraction column (Waters), following instructions provided by the vendor. Briefly, after the activation and equilibration of the column resin with 500 μL of 3% acetonitrile and 0.1% formic acid, peptides were loaded onto the column. After desalting peptides, a total of eight fractions of peptides were collected by eluting the sample with 500 μL of 0.1% triethylamine solution with increasing acetonitrile concentration (namely, 5.0, 7.5, 10.0, 12.5, 15.0, 17.5, 20.0, and 50.0%). Each fraction was dried under a vacuum before analysis by high-resolution spectrometry coupled to liquid chromatography (nanoLC-MS/MS) analysis.

Sample Acquisition for the Creation of the Ion Library. For nanoLC-MS/MS analysis, each fraction of peptides was dissolved in 150 μL of 3% acetonitrile + 0.1% formic acid. We analyzed 5 μL of each fraction (roughly corresponding to 2.5 μg of peptides) on a 5600+ TripleTOF instrument, working in nanospray mode with a NANOSpray III ion source (SCIEX) coupled to a nanoACQUITY LC system (Waters). Peptides were loaded and desalted on an ACQUITY C18 trapping column (180 μm × 20 mm, Waters) for 4 min at a 4.0 μL/min flow rate (1% acetonitrile + 0.1% formic acid) and then separated on a PicoFrit C18 column (75 μm × 25 cm, New Objective Inc.). Peptides were eluted with a 2 h linear gradient at 300 nL/min (from 3 to 45% acetonitrile in water + 0.1% formic acid); the column was washed with 90% acetonitrile and then equilibrated for 18 min to 3% acetonitrile.

Data-dependent acquisition (DDA) spectra were collected over the 2 h gradient. Peptides with charge states 2+ to 5+ showing an intensity higher than 150 counts were selected as precursors for tandem mass spectrometry (MS/MS) acquisition. A survey spectrum (400−1250) was acquired for 250 ms, followed by 40 DDA MS/MS experiments (100−1500 *m*/*z*, 100 ms of accumulation time each).

Data Analysis for Protein Identification. Raw DDA data from nanoLC-MS/MS were analyzed with ProteinPilot software (SCIEX), using the Paragon algorithm.[19] All DDA spectra were searched against a reviewed *Rattus norvegicus* database reporting 8131 proteins and downloaded as FASTA file from UniProt[20] on February 25th, 2019. A false discovery rate[21] analysis was performed against a decoy version of the same database. Identifications at 1% false discovery rate at the spectrum level were retained, with a minimum threshold of 90% in peptide confidence. Only nonshared peptides were used to build the ion library.

Sequential Window Acquisition of All Theoretical Mass Spectra for Protein Quantification. Tryptic peptides (1.66 μg) from each sample were analyzed for protein quantification, following a label-free sequential window acquisition of all theoretical mass spectra (SWATH) protocol.[22] For SWATH acquisitions, peptides were loaded on the chromatographic column with the same liquid chromatography method used for protein identification. Mass spectrometry parameters were set as follows: precursor ion selection was done in the 400−1250 *m*/*z* range, with a variable window width strategy (7 to 50 Da). After a full-range survey scan of 250 ms, 100 consecutive SWATH experiments (100−1500 *m*/*z*) were performed, each lasting 25 ms.

Raw Data Analysis. Raw data for protein quantification were searched against our new ion library. For quantification, the following criteria were used: minimum peptide confidence 90%, 50 ppm maximum mass tolerance, 30 min maximum retention time tolerance, six parent-to-fragment transitions per peptide, and modified peptides were not allowed. Raw data were imported in MarkerView software (SCIEX) and normalized with the most likely ratio method.[23] Normalized data were preprocessed with logarithm weighting and Pareto scaling.[24]

Principal component analysis (PCA) was performed on the processed data. Since PCA indicated the second replicate of the control group (sample 2) as an outlier, we decided to exclude it from subsequent statistics on proteomics data and in general from downstream analyses.

For statistical analysis, one-to-one comparisons were performed using an unpaired, two-tailed *t*-test, considering a *p*-value <0.05 as significant. Moreover, according to the resulting *t*-value, significantly dysregulated proteins, which we refer to as differentially represented proteins (DRPs), were classified as either up- or down-regulated.

Bioinformatics and Comparisons with Our Previous Space Study. Our past ISS study featured, for the two experimental variables space and NC, four experimental classes, namely, samples on land without NC treatment (ground−), in space without NC treatment (ISS−), on land with NC treatment (ground+), and in space with NC treatment (ISS+). Two DEGs were at the intersection between comparisons ground+ vs ground− and ISS+ vs ISS−, both studying NC effects. However, few genes passed statistical requirements for the latter comparison, which contained a mere nine DEGs. Therefore, we expected ground+ vs ground− to be more informative. The current proteomics experiment is dedicated to the investigation of the biological alterations brought about by NC on muscle cells. As such, it contains two experimental classes, namely, sample with (+) or without (−) NC treatment, and a single possible comparison, ground+ vs ground−.

https://doi.org/10.1021/acsomega.3c09715
ACS Omega 2024, 9, 29226−29233

Through local scripting, we clustered hierarchically both samples and DRPs based on protein quantifications, visualizing the results as a cluster heat map. DRPs were charted in a volcano plot, as well. We also prepared Venn diagrams distributing gene/protein names in ground+ vs ground− (proteomics), ground+ vs ground− (transcriptomics), and ISS + vs ISS− (transcriptomics). We identified shared factors among the two studies and performed gene ontology (GO) to qualify, for selected subsets, the effects of NC in terms of biological processes, molecular functions, or cellular components. GO analyses were performed with GOrilla,[25] run in target-and-background-list mode. Background files were either a list of all rat genes, retrieved via Ensembl BioMart,[26,27] or a narrower subset of rat gene names flagged as "stable" by Ensembl itself.[28] Significance thresholds for p- and q-values were both set at 0.05. Significant GOrilla results were graphically summarized as scatter plots, using REVIGO[29] and Cytoscape 3.10.2.[30]

RESULTS AND DISCUSSION

Dynamic light scattering analyses defined, for NC preparations, HD at 189.5 ± 2.212 nm, PDI at 0.179 ± 0.033, and ζ-potential at −19.3 ± 2.328 mV, indicative of high colloidal stability. TEM evidenced thin conformal FBS coating on NPs after negative contrast. Such characterizations are reported in Figure S1.

Cultures invariably survived until the end of the experiment; the measured temperature profile, followed by the incubator, matched our ISS standard satisfactorily (data not shown). Following protein extraction, each sample yielded an overall protein mass of at least 600 μg, as shown in Table S1. Except for the second replicate of the control group (sample 2), samples were segregated according to their class of origin on a PCA score plot (Figure S2). The deviant sample was excluded from further analyses.

After all filtering steps, our protein identification pipeline restituted a new ion library containing 1907 proteins. Label-free SWATH quantified, with the chosen parameters, 1655 proteins present in all the samples, and statistical analyses across experimental classes highlighted 137 DRPs, of which 60 up- and 77 down-regulated (Table S2). As expected, hierarchical clustering on such proteins across samples organizes the samples according to NC treatment (Figure 1).

Venn intersections between gene identifiers for DRPs and DEGs for NC-investigating comparisons in our previous ISS study, i.e., transcriptomics ground+ vs ground− and ISS+ vs ISS−, found no shared genes among the three (Figure 2). This is not particularly surprising, as comparison ISS+ vs ISS− was composed of only nine elements. Conversely, the two comparisons on land have four genes in common, namely, *guanine nucleotide-binding protein-like 3* (*Gnl3*), *histone cluster 1 H4 family member b* (*Hist1h4b*), *metadherin* (*Mtdh*, also known as *astrocyte elevated gene 1*, *AEG-1*), and *thyroid hormone receptor interactor 12* (*Trip12*). All four factors display a "coherent" up- or downtrend, in the sense that each of them is either up- (*Hist1h4b*) or down-regulated (*Gnl3*, *Mtdh*, *Trip12*) in both parent sets (Figures 2 and 3). The four, united with the two coherent genes identified for NC in our orbital investigation (*Lmna* and *H2afx*), were our focus for GO investigations. We collectively refer to them as the "coherent set".

As we did not observe substantial differences when using all rat vs stable-only rat gene identifiers as background sets for

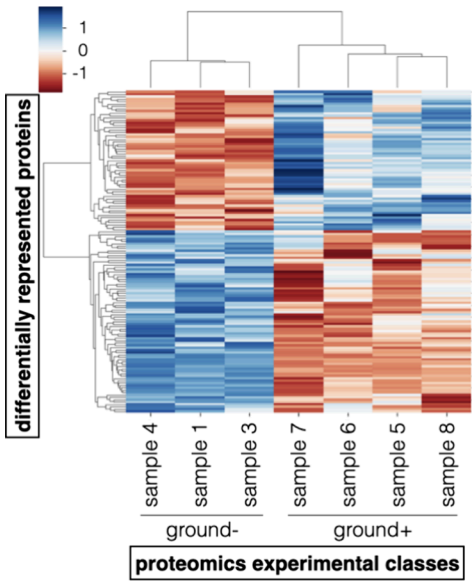

Figure 1. Proteomics cluster heat map. Differentially represented proteins (DRPs) are hierarchically clustered based on their quantifications across samples, which are also hierarchically clustered according to their DRP quantification profile. For each DRP, a heat map reports quantification values, which are negative for down-regulation (in cyan) and positive for up-regulation (in red; see also the color legend on top, left). Hierarchical clustering correctly identifies nanoceria-treated (ground+) samples and untreated (ground−) samples as two separate groups.

GO, we disregarded the first for the investigations presented hereafter. GO analyses of cellular components on DRPs for ground+ vs ground, either irrespective of up/down trends or focusing on up- and down-regulated protein subsets separately, support an overall involvement of vesicular networks and ribonuclear complexes. The latter is held up by an array of GO terms essentially relating to nucleolus/ribosome or to nucleosome (Figure 2). For the same DRP sets, relevantly enriched GO biological processes generally pertain to protein synthesis/metabolism in response to stimuli, as well as to nucleosome/ribonucleoprotein complex organization. Analyses of GO molecular functions yield somewhat reduced but consistent results, which point to interactions between nucleic acids and proteins, perhaps with some emphasis on RNA (Figure S3). The coherent set shows significant enrichment for GO cellular components. GO terms associated with coherent genes tend to relate to the nuclear compartment, and particularly to the nucleosome (Figure 2). The genes with the most obvious connections to nucleosomes or DNA packaging are *H2afx* and *Hist1h4b*. Coding for histone isoforms, they produce direct components of nucleosomes.[31−34] As a lamin, Lmna contacts both the nuclear lamina, DNA, and proteins associated with it.[35,36] Gnl3 is a nuclear factor too,[32,33] and it is found together with nucleolar chromatin-bound tumor protein 53 (tp53), a pivotal and well-studied keeper of DNA integrity.[37] Intriguingly, Trip12 is also an important regulator of the response against DNA damage and interacts with both H2afx and tp53, specifically by confining ubiquitinated histone 2A (H2A)/H2afx at damaged DNA sites and by regulating cyclin-dependent kinase inhibitor 2A (cdkn2a), an activator of tp53.[35,36] Gnl3 is a nucleolar GPTase, believed to be crucial for ribosomal RNA processing and, as Trip12, thought to control tp53 by stabilizing murine

https://doi.org/10.1021/acsomega.3c09715
ACS Omega 2024, 9, 29226−29233

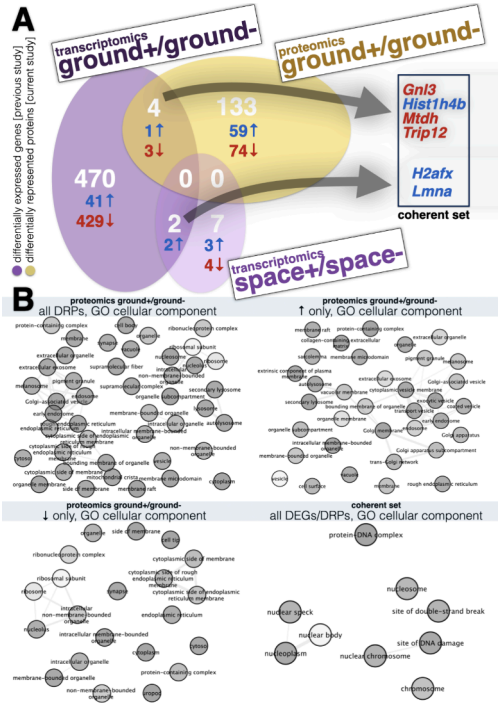

Figure 2. Proteomics results and their implications for our previous space investigation of nanoceria (NC). (A) Venn diagrams comparing gene/protein names for our set of differentially represented proteins (DRPs, proteomics ground+/ground−) to NC-investigating comparisons of our previous transcriptomics study, performed partially aboard the International Space Station (transcriptomics space +/space−) and partially on land (transcriptomics ground +/ground−). + and − in comparison names stand for, respectively, with or without NC treatment, and/stands for vs. Each subset reports the general number of differentially represented proteins/differentially expressed genes (in white) and the internal composition in terms of up- (↑, blue) or down-regulation (↓, red). Genes at the intersection of two parent sets are invariably "coherent", meaning that they are systematically either up- or down-regulated. The identity of coherent genes at each of two intersection is reported on the right (gray panels, blue for up-regulated factors, red for down-regulated ones). (B) Scatter plots for gene ontology (GO) analyses, showing significant GO-term enrichment for GO cellular components, using as input DRPs in ground+/ground−—either all of them, up-regulated (↑)-only, or down-regulated (↓)-only—or the six shortlisted DRPs/differentially expressed genes (DEGs) within the "coherent set". GO-term color saturation (gray circles) reflects statistical robustness (the darker the color, the lower the associated *p*-value). Gray lines are connecting semantically close GO terms; their width positively correlates with the amount of resemblance. More generally, GO terms are roughly positioned according to their meaning, but their layout was modified whenever needed to fit graphical constraints.

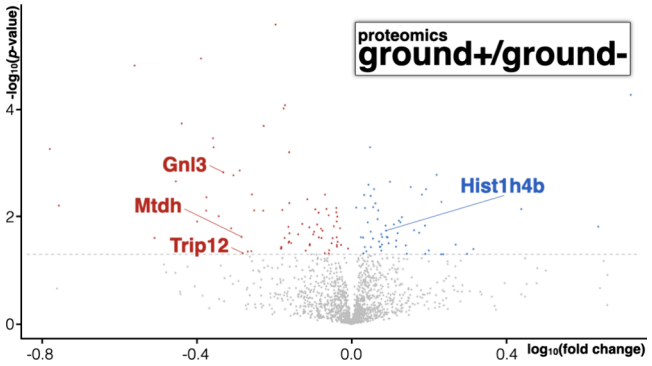

Figure 3. Volcano plot of all proteins in our proteomics data set. Below a 0.05 threshold for *p*-value (∼ −1.3 in logarithmic scale, gray dashed line), differentially represented proteins for nanoceria-treated (ground+) vs untreated samples (ground−) are reported as red (if down-regulated) or blue (if up-regulated) points. All remaining proteins are depicted as gray points. Gene/protein names are reported for our "coherent" factors, namely, those shared with a previous transcriptomics nanoceria study and systematically either up- or down-regulated.

double minute 2 (Mdm2) in the nucleus. Gnl3 is also a negative regulator of protein ubiquitination; concerning DNA stability, it contributes to telomere maintenance.[38] *Mtdh* is in turn a proto-oncogene for multiple cancer types. It codes for a direct interactor of Mdm2 and can promote cell proliferation via Mdm2-tp53-dependent mechanisms.[37,38]

Being the result of independent omics experiments, and with a seemingly consistent involvement in DNA packaging/preservation, coherent factors offer novel insight on the molecular dynamics through which NC acts against OS. Together with antioxidant effects, in addition, such factors seem to indicate an antiproliferative effect of NC on cells. The excellent redox characteristics of NC, conferring it autoregenerative radical-scavenging capabilities,[39] make it an appealing antioxidant drug candidate, particularly when long duration and low administration rate are desirable. In addition, the activity of NC is bimodal: depending on local chemical conditions, it can operate as an antioxidant or as a prooxidant. At physiological pH, NC behaves as an antioxidant, protecting cells from OS. Conversely, in acidic pH, it acts as a prooxidant,[40,41] and that may represent a further advantage whenever selective toxicity in acidic microenvironments is beneficial, as in several pathological conditions, including cancer.[42]

Consistent with our findings, Datta and colleagues demonstrated that NC treatment of colorectal carcinoma cells increases the cellular content of phosphorylated H2afx, notably recognized as a marker of DNA damage, activating the tumor-suppressor tp53. Researchers found that—upon NC exposure—an increased ROS concentration causes DNA double-strand breaks, leading to H2afx phosphorylation, which in turn activates tp53 and consequently caspases 3/9, eventually resulting in tumor cell apoptosis.[43] Other investigations have been carried out to understand if and how NC interacts with DNA. Recent research supports a direct affinity between NC and DNA, with NC that adsorbs DNA by adhering to its phosphate/sugar backbone regardless of its primary sequence, leading to the formation of a DNA corona.[44−47] Steric interactions between inorganic NPs and DNA have been investigated *in vitro*, and some proposed DNA can wrap around NPs similarly to what happens with histones in the formation of nucleosomes. In addition, since phosphorylated molecules are omnipresent in biological systems, the catalytic role of NC was exploited in a nucleotide-relevant reaction, namely, phosphate-ester hydrolysis.[44] In biological conditions, however, NC should bind rather than hydrolyze DNA, as suggested by studies on plasmids.[48,49] In any case—be the action of NC on DNA either direct or indirect—the nuclear/nucleosome involvement emphasized by our work appears to be coherent with existing literature and fits with our past tests aboard the ISS.[17]

Albeit our current focus is rat, further investigations from our group were concerned with assessing the therapeutic

https://doi.org/10.1021/acsomega.3c09715
ACS Omega 2024, 9, 29226−29233

potential of NC in space using either mouse myoblasts or planarian worms. Mouse myoblasts were cultured on the ISS or on land, with or without NC, and their transcriptome was evaluated while they were proliferating. There, NC elicited little transcriptional variations and no statistically supported GO annotations, possibly due to the particularly challenging experimental design, which involved a timely administration of NC to cells in their active proliferation phase.[50] Instead, in X-ray-treated planarians, we could determine—among other things—that NC reduces cell death and prevents DNA fragmentation.[51]

CONCLUSIONS

NC owns a wide range of well-characterized physicochemical properties, depending on synthesis method, size, shape, and coating. These can be adjusted to various purposes, such as industrial processes like catalysis, chemo-mechanical polishing, solid oxide fuel cells, and sensing.[52] NC has also been exploited in several biomedical areas, including regenerative medicine, neuroprotection, and photoreceptor protection, as well as in the regulation of metabolism (*e.g.*, diabetes and obesity).[40] The molecular underpinnings of NC efficacy as a drug are thought to depend, to a significant extent, on pronounced antioxidant properties. Yet, the exact mechanisms of its action on cell metabolism are largely uncharacterized.[39−49,17,50,51]

Our proteomics helped highlight an increased presence of histone Hist1h4b on NC-treated samples, hinting that the NP can alter nucleosome state/formation. The current data set further strengthens this idea by pointing out a response from other nuclear factors and molecules responsive to DNA damage, like Gnl3 and Trip12, which exert control over the cell cycle too. Mtdh promotes instead cell division and progression of several types of tumors, also by activation of matrix metalloproteinase-9 (Mmp9). This is an enzyme that participates in angiogenesis and stromal remodeling, thus initiating metastatic processes.[53] Interestingly, the protein is found at nuclear and perinuclear regions.[53−55]

This investigation extends a previous study of NC on muscle cells to counteract OS in space, a place in which long-lasting antioxidant activity is especially desired. In agreement with published evidence, shortlisted genes/proteins putatively mediating the molecular action of NC are mainly active in the cell nucleus, where they protect chromatin and modulate the cell cycle.

ASSOCIATED CONTENT

Data Availability Statement

Mass spectrometry proteomics data have been deposited to the ProteomeXchange Consortium via the PRoteomics IDEntifications (PRIDE) partner repository[56] (data set identifier: PXD047391). All other relevant data are included in the manuscript or its Supporting Information.

Supporting Information

The Supporting Information is available free of charge at https://pubs.acs.org/doi/10.1021/acsomega.3c09715.

Characterization of nanoceria; principal component analysis score plot; scatter plots for gene ontology analyses; total protein quantification; differentially represented proteins for nanoceria-treated with respect to untreated samples (PDF)

AUTHOR INFORMATION

Corresponding Authors

Andrea Degl'Innocenti − *Smart Bio-Interfaces, Center for Materials Interfaces, Istituto Italiano di Tecnologia, Pontedera, Pisa 56025, Italy; Department of Medical Biotechnologies, Polyclinic Hospital Santa Maria alle Scotte, Università degli Studi di Siena, Siena 53100, Italy;* orcid.org/0000-0002-5204-5601; Email: andrea.deglinnocenti@iit.it

Andrea Armirotti − *Analytical Chemistry Facility, Istituto Italiano di Tecnologia, Genova 16163, Italy;* orcid.org/0000-0002-3766-8755; Email: andrea.armirotti@iit.it

Gianni Ciofani − *Smart Bio-Interfaces, Center for Materials Interfaces, Istituto Italiano di Tecnologia, Pontedera, Pisa 56025, Italy;* orcid.org/0000-0003-1192-3647; Email: gianni.ciofani@iit.it

Authors

Clarissa Braccia − *Analytical Chemistry Facility, Istituto Italiano di Tecnologia, Genova 16163, Italy*

Giada Graziana Genchi − *Smart Bio-Interfaces, Center for Materials Interfaces, Istituto Italiano di Tecnologia, Pontedera, Pisa 56025, Italy; Department of Biosciences, Biotechnologies and Biopharmaceutics, Università degli Studi di Bari Aldo Moro, Bari 70125, Italy*

Nicoletta di Leo − *Smart Bio-Interfaces, Center for Materials Interfaces, Istituto Italiano di Tecnologia, Pontedera, Pisa 56025, Italy*

Luca Leoncino − *Electron Microscopy Facility, Istituto Italiano di Tecnologia, Genova 16163, Italy;* orcid.org/0000-0001-8561-3460

Federico Catalano − *Electron Microscopy Facility, Istituto Italiano di Tecnologia, Genova 16163, Italy;* orcid.org/0000-0001-5574-0063

Complete contact information is available at: https://pubs.acs.org/10.1021/acsomega.3c09715

Author Contributions

[#]A.D.I. and C.B. contributed equally to this study as co-first authors.

Author Contributions

[▽]G.G.G. and N.d.L. contributed equally to this study as co-second authors.

Notes

The authors declare no competing financial interest.

ACKNOWLEDGMENTS

This work received support from the Italian Space Agency (ASI) [grant number 2016-7-U.0].

NOMENCLATURE

DDA=data-dependent acquisition
DEG=differentially expressed gene
DMEM=Dulbecco's modified Eagle's medium
DRP=differentially represented protein
FBS=fetal bovine serum
GO=gene ontology
HD=hydrodynamic diameter
ISS=International Space Station
MS/MS=tandem mass spectroscopy
nanoLC-MS/MS=nano mass spectrometry coupled to liquid chromatography

https://doi.org/10.1021/acsomega.3c09715
ACS Omega 2024, 9, 29226−29233

NC=nanoceria
NP=nanoparticle
OS=oxidative stress
PCA=principal component analysis
PDI=polydispersity index
Pen/Strep=100 U/mL penicillin−100 μg/mL streptomycin
PRIDE=PRoteomics IDEntifications
RIPA=radioimmunoprecipitation assay buffer
ROS=reactive oxygen species
SWATH=sequential window acquisition of all theoretical mass spectra
TEM=transmission electron microscopy

REFERENCES

(1) Valko, M.; Leibfritz, D.; Moncol, J.; Cronin, M. T. D.; Mazur, M.; Telser, J. Free radicals and antioxidants in normal physiological functions and human disease. *Int. J. Biochem. Cell Biol.* **2007**, *39* (1), 44−84.

(2) Senoner, T.; Dichtl, W. Oxidative stress in cardiovascular diseases: Still a therapeutic target? *Nutrients* **2019**, *11* (9), 2090.

(3) Vatner, S. F.; Zhang, J.; Oydanich, M.; Berkman, T.; Naftalovich, R.; Vatner, D. E. Healthful aging mediated by inhibition of oxidative stress. *Ageing Res. Rev.* **2020**, *64*, No. 101194.

(4) Gomes, M. J.; Martinez, P. F.; Pagan, L. U.; et al. Skeletal Muscle Aging: Influence of Oxidative Stress and Physical Exercise. *Oncotarget* **2017**, *8*, 20428.

(5) Islam, M. T. Oxidative stress and mitochondrial dysfunction-linked neurodegenerative disorders. *Neurol Res.* **2017**, *39* (1), 73−82.

(6) Matés, J. M.; Sánchez-Jiménez, F. M. Role of reactive oxygen species in apoptosis: implications for cancer therapy. *Int. J. Biochem. Cell Biol.* **2000**, *32* (2), 157−170.

(7) Liguori, I.; Russo, G.; Curcio, F.; et al. Oxidative stress, aging, and diseases. *Clin Interv Aging.* **2018**, *13*, 757−772.

(8) Nordberg, J.; Arnér, E. S. J. Reactive oxygen species, antioxidants, and the mammalian thioredoxin system. *Free Radic Biol. Med.* **2001**, *31* (11), 1287−1312.

(9) Schallreuter, K. U.; Moore, J.; Wood, J. M.; et al. In vivo and in vitro evidence for hydrogen peroxide (H2O2) accumulation in the epidermis of patients with vitiligo and its successful removal by a UVB-activated pseudocatalase. *J. Invest. Dermatol. Symp. Proc.* **1999**, *4*, 91−96.

(10) Abdel-Mageed, H. M.; El-Laithy, H. M.; Mahran, L. G.; Fahmy, A. S.; Mäder, K.; Mohamed, S. A. Development of novel flexible sugar ester vesicles as carrier systems for the antioxidant enzyme catalase for wound healing applications. *Process Biochemistry.* **2012**, *47* (7), 1155−1162.

(11) Davoodbasha, M. A.; Park, B. R.; Rhee, W. J.; Lee, S. Y.; Kim, J. W. Antioxidant potentials of nanoceria synthesized by solution plasma process and its biocompatibility study. *Arch. Biochem. Biophys.* **2018**, *645*, 42−49.

(12) Li, C.; Shi, X.; Shen, Q.; Guo, C.; Hou, Z.; Zhang, J. Hot topics and challenges of regenerative nanoceria in application of antioxidant therapy. *J. Nanomater.* **2018**, *2018*, 1.

(13) Niu, J.; Azfer, A.; Rogers, L. M.; Wang, X.; Kolattukudy, P. E. cardioprotective effects of cerium oxide nanoparticles in a transgenic murine model of cardiomyopathy. *Cardiovasc. Res.* **2007**, *73* (3), 549−559.

(14) Das, S.; Singh, S.; Dowding, J. M.; et al. The induction of angiogenesis by cerium oxide nanoparticles through the modulation of oxygen in intracellular environments. *Biomaterials.* **2012**, *33* (31), 7746−7755.

(15) Augustine, R.; Dalvi, Y. B.; Dan, P.; et al. nanoceria Can Act as the Cues for Angiogenesis in Tissue-Engineering Scaffolds: Toward Next-Generation in Situ Tissue Engineering. *ACS Biomater Sci. Eng.* **2018**, *4* (12), 4338−4353.

(16) Karakoti, A. S.; Monteiro-Riviere, N. A.; Aggarwal, R.; et al. nanoceria as antioxidant: Synthesis and biomedical applications. *JOM.* **2008**, *60* (3), 33−37.

(17) Genchi, G. G.; Degl'Innocenti, A.; Salgarella, A. R.; et al. Modulation of gene expression in rat muscle cells following treatment with nanoceria in different gravity regimes. *Nanomedicine.* **2018**, *13* (22), 2821−2833.

(18) Wang, H.; Sun, S.; Zhang, Y.; Chen, S.; Liu, P.; Liu, B. An off-line high pH reversed-phase fractionation and nano-liquid chromatography-mass spectrometry method for global proteomic profiling of cell lines. *J. Chromatogr B Analyt Technol. Biomed Life Sci.* **2015**, *974*, 90−95.

(19) Shilov, I. V.; Seymourt, S. L.; Patel, A. A.; et al. The paragon algorithm, a next generation search engine that uses sequence temperature values sequence temperature values and feature probabilities to identify peptides from tandem mass spectra. *Mol. Cell. Proteomics* **2007**, *6* (9), 1638−1655.

(20) http://www.uniprot.org/proteomes/ UP000002494.

(21) Tang, W. H.; Shilov, I v.; Seymour, S. L. Nonlinear Fitting Method for Determining Local False Discovery Rates from Decoy Database Searches. *J. Proteome Res.* **2008**, *7* (9), 3661−3667.

(22) Collins, B. C.; Hunter, C. L.; Liu, Y.; et al. Multi-laboratory assessment of reproducibility, qualitative and quantitative performance of SWATH-mass spectrometry. *Nat. Commun.* **2017**, *8* (1), 291 DOI: 10.1038/s41467-017-00249-5.

(23) Lambert, J. P.; Ivosev, G.; Couzens, A. L.; et al. Mapping differential interactomes by affinity purification coupled with data-independent mass spectrometry acquisition. *Nat. Methods.* **2013**, *10* (12), 1239−1245.

(24) van den Berg, R. A.; Hoefsloot, H. C.; Westerhuis, J. A.; Smilde, A. K.; van der Werf, M. J. Centering, scaling, and transformations: Improving the biological information content of metabolomics data. *BMC Genomics* **2006**, *7*, 142.

(25) Eden, E.; Navon, R.; Steinfeld, I.; Lipson, D.; Yakhini, Z. GOrilla: A tool for discovery and visualization of enriched GO terms in ranked gene lists. *BMC Bioinf.* **2009**, *10*, 48.

(26) Smedley, D.; Haider, S.; Ballester, B.; et al. BioMart - Biological queries made easy. *BMC Genomics* **2009**, *10*, 22.

(27) Kinsella, R. J.; Kähäri, A.; Haider, S.; et al. Ensembl BioMarts: A hub for data retrieval across taxonomic space. *Database* **2011**, *2011*, bar030.

(28) Cunningham, F.; Allen, J. E.; Allen, J.; et al. Ensembl 2022. *Nucleic Acids Res.* **2022**, *50* (D1), D988−D995.

(29) Supek, F.; Bošnjak, M.; Škunca, N.; Šmuc, T.; Gibas, C. Revigo summarizes and visualizes long lists of gene ontology terms. *PLoS One* **2011**, *6* (7), No. e21800.

(30) Franz, M.; Lopes, C. T.; Fong, D.; et al. Cytoscape.js 2023 update: a graph theory library for visualization and analysis. *Bioinformatics* **2023**, *39* (1), btad031 DOI: 10.1093/bioinformatics/btad031.

(31) Sedelnikova, O. A.; Pilch, D. R.; Redon, C.; Bonner, W. M. Histone H2AX in DNA Damage and Repair. *Cancer Biol. Ther.* **2003**, *2*, 233.

(32) Fernandez-Capetillo, O.; Lee, A.; Nussenzweig, M.; Nussenzweig, A. H2AX: The histone guardian of the genome. *DNA Repair (Amst).* **2004**, *3* (8−9), 959−967.

(33) Turner, B. M. Histone H4, the cell cycle and A question of integrity. *BioEssays.* **1995**, *17* (12), 1013−1015.

(34) Kumar, K.; Moirangthem, R.; Kaur, R. Genome protection: histone H4 and beyond. *Curr. Genet.* **2020**, *66* (5), 945−950.

(35) Dittmer, T.; Misteli, T. The Lamin Protein Family. *Genome Biol.* **2011**, *12*, 222.

(36) Worman, H. J. Nuclear lamins and laminopathies. *Journal of Pathology.* **2012**, *226* (2), 316−325.

(37) Harris, C. C. Structure and Function of the P53 Tumor Suppressor Gene: Clues for Rational Cancer Therapeutic Strategies. *J. Natl. Cancer Inst.* **1996**, *88*, 1442.

(38) Ma, H.; Pederson, T. Nucleostemin: a multiplex regulator of cell-cycle progression. *Trends Cell Biol.* **2008**, *18* (12), 575−579.

(39) Thakur, N.; Manna, P.; Das, J. Synthesis and biomedical applications of nanoceria, a redox active nanoparticle. *J. Nanobiotechnol.* **2019**, *17* (1), 84 DOI: 10.1186/s12951-019-0516-9.

https://doi.org/10.1021/acsomega.3c09715
ACS Omega 2024, 9, 29226−29233

(40) Saifi, M. A.; Seal, S.; Godugu, C. nanoceria, the versatile nanoparticles: Promising biomedical applications. *J. Controlled Release* **2021**, *338*, 164−189.
(41) Kailashiya, J.; Dash, D. nanoceria and Its Biomedical Relevance. *Ann. Natl. Acad. Med. Sci.* **2019**, *55* (01), 014−017.
(42) Tang, J. L. Y.; Moonshi, S. S.; Ta, H. T. nanoceria: an innovative strategy for cancer treatment. *Cell. Mol. Life Sci.* **2023**, *80* (2), 46 DOI: 10.1007/s00018-023-04694-y.
(43) Datta, A.; Mishra, S.; Manna, K.; Das, S. K.; Mukherjee, S.; Roy, S. Pro-Oxidant Therapeutic Activities of Cerium Oxide Nanoparticles in Colorectal Carcinoma Cells. *ACS Omega* **2020**, *5* (17), 9714−9723.
(44) Pautler, R.; Kelly, E. Y.; Huang, P. J. J.; Cao, J.; Liu, B.; Liu, J. Attaching DNA to nanoceria: Regulating oxidase activity and fluorescence quenching. *ACS Appl. Mater. Interfaces.* **2013**, *5* (15), 6820−6825.
(45) Liu, B.; Sun, Z.; Huang, P. J. J.; Liu, J. Hydrogen peroxide displacing DNA from nanoceria: Mechanism and detection of glucose in serum. *J. Am. Chem. Soc.* **2015**, *137* (3), 1290−1295.
(46) Griffith, D. M.; Jayaram, D. T.; Spencer, D. M.; Pisetsky, D. S.; Payne, C. K. DNA-nanoparticle interactions: Formation of a DNA corona and its effects on a protein corona. *Biointerphases* **2020**, *15* (5), No. 051006, DOI: 10.1116/6.0000439.
(47) Vlasova, N.; Markitan, O. Phosphate−nucleotide−nucleic acid: Adsorption onto nanocrystalline ceria surface. *Colloids Surf., A* **2022**, *648*, No. 129214.
(48) Kuchma, M. H.; Komanski, C. B.; Colon, J.; et al. Phosphate ester hydrolysis of biologically relevant molecules by cerium oxide nanoparticles. *Nanomedicine.* **2010**, *6* (6), 738−744.
(49) Yokel, R. A.; Hussain, S.; Garantziotis, S.; Demokritou, P.; Castranova, V.; Cassee, F. R. The yin: An adverse health perspective of nanoceria: Uptake, distribution, accumulation, and mechanisms of its toxicity. *Environ. Sci. Nano.* **2014**, *1* (5), 406−428.
(50) Genchi, G. G.; Degl'Innocenti, A.; Martinelli, C.; et al. Cerium oxide nanoparticle administration to skeletal muscle cells under different gravity and radiation conditions. *ACS Appl. Mater. Interfaces* **2021**, *13* (34), 40200−40213.
(51) Salvetti, A.; Gambino, G.; Rossi, L.; et al. Stem cell and tissue regeneration analysis in low-dose irradiated planarians treated with cerium oxide nanoparticles. *Materials Science and Engineering: C* **2020**, *115*, No. 111113.
(52) Andreescu, D.; Bulbul, G.; Özel, R. E.; Hayat, A.; Sardesai, N.; Andreescu, S. Applications and implications of nanoceria reactivity: Measurement tools and environmental impact. *Environ. Sci. Nano.* **2014**, *1* (5), 445−458.
(53) Dhiman, G.; Srivastava, N.; Goyal, M.; et al. metadherin: A therapeutic target in multiple cancers. *Front. Oncol.* **2019**, *9*, 349 DOI: 10.3389/fonc.2019.00349.
(54) Kang, D. C.; Su, Z. Z.; Sarkar, D.; Emdad, L.; Volsky, D. J.; Fisher, P. B. Cloning and characterization of HIV-1-inducible astrocyte elevated gene-1, AEG-1. *Gene.* **2005**, *353* (1), 8−15.
(55) Chen, Y.; Huang, S.; Guo, R.; Chen, D. metadherin-mediated mechanisms in human malignancies. *Biomark Med.* **2021**, *15* (18), 1769−1783.
(56) Perez-Riverol, Y.; Bai, J.; Bandla, C.; et al. The PRIDE database resources in 2022: a hub for mass spectrometry-based proteomics evidences. *Nucleic Acids Res.* **2022**, *50* (D1), D543−D552.

https://doi.org/10.1021/acsomega.3c09715
ACS Omega 2024, 9, 29226−29233